Bose-Einstein Condensation of Photons in a Four-Site Quantum Ring

Andreas Redmann ⬤,* Christian Kurtscheid ⬤,† Niels Wolf ⬤, Frank Vewinger ⬤, Julian Schmitt ⬤, and Martin Weitz ⬤
Institut für Angewandte Physik, Universität Bonn, Wegelerstrasse 8, 53115 Bonn, Germany

Thermalization of radiation by contact to matter is a well-known concept, but the application of thermodynamic methods to complex quantum states of light remains a challenge. Here, we observe Bose-Einstein condensation of photons into the hybridized ground state of a coupled four-site ring potential. In our experiment, the periodically closed ring lattice superimposed by a weak harmonic trap for photons is realized inside a spatially structured dye-filled microcavity. Photons thermalize to room temperature, and above a critical photon number macroscopically occupy the symmetric linear combination of the site eigenstates with zero phase winding, which constitutes the ground state of the system. The mutual phase coherence of photons at different lattice sites is verified by optical interferometry.

Populating the ground state of complex systems by freezing out thermal excitations is at the core of many low-temperature quantum phenomena that involve correlated many-body states, such as fractional quantum Hall or spin-charge separated states [1,2]. A tailoring of correlated quantum states has also been achieved with cold atoms in optical lattice potentials, e.g., to realize effects known from solid state physics as the Mott-insulator transition [3]. An accumulation into the ground state in the periodic potential is here achieved by adiabatic loading of cold atoms into the lattice potential.

A different route to study many-body physics by direct cooling has recently been explored in the field of optical physics. Studies in this domain have long been restricted to nonequilibrium phenomena as coupled laser systems [4,5], but more recent work has realized thermalization of low-dimensional optical quantum gases, e.g., in exciton-polariton gases by interparticle collisions [6,7] and in photon gases by contact to an equilibrium reservoir [8–10], opening new ways of cooling directly into nontrivial many-body states. The latter have been demonstrated to allow for a thermodynamic phase transition of photons to a macroscopically occupied ground state, the Bose-Einstein condensate. Corresponding experiments have been carried out in dye-filled optical microcavities [8,11–13], erbium-doped fibers [14], plasmonic lattices [15], and more recently in semiconductor microcavities [16,17]. Furthermore, theoretical work has suggested Bose-Einstein condensation of photons in a microcavity plasma [18]. Such light-matter platforms open the possibility to engineer

quantum states of light by energetic selection [19], while state preparation methods based on the competition between gain and loss are limited to classical physics phenomena [20,21]. In a recent experiment, the thermalization of light in a double well potential to populate the "bonding" ground state of this optical analog of a dimer molecule has been demonstrated [22]. On the way to more complex systems, lattice potentials have been realized with both photon and polariton systems [23–25]. With polaritons, both thermalization to the bottom edge of a tilted ring structure as well as multimode condensation into coupled states of opposite orbital flow in a ring have been investigated [26–28].

In this Letter, we report measurements of the thermalization and Bose-Einstein condensation of a two-dimensional photon gas to the ground state of a periodically closed ring lattice, where the notation of a phase winding becomes meaningful. The four-site ring is superimposed by a harmonic trapping potential and is realized by imprinting a corresponding surface structure on one of the cavity mirrors of a dye-filled optical microcavity. The photon gas thermalizes to room temperature by repeated absorption and emission on the dye molecules. Above a critical photon number, we observe a macroscopic fraction of photons occupying the linear combination of eigenfunctions with zero phase winding, which constitutes the energetic ground state of the system. This is accompanied by a saturation of the population in the excited modes, as expected for the phase transition to a Bose-Einstein condensate. The photons delocalize over the ring structure and the obtained fixed phase relation between photons from different lattice sites is verified by optical interferometry.

The used dye microcavity platform shown in Fig. 1(a) confines photons between two highly reflecting mirrors of reflectivity above 99.997%, where the cavity volume is filled with a Rhodamine 6G dye solution of 1 mmol/l

---

*Contact author: redmann@iap.uni-bonn.de
†Present address: Fraunhofer-Institut für Hochfrequenzphysik und Radartechnik FHR, Fraunhoferstr. 20, 53343 Wachtberg, Germany.
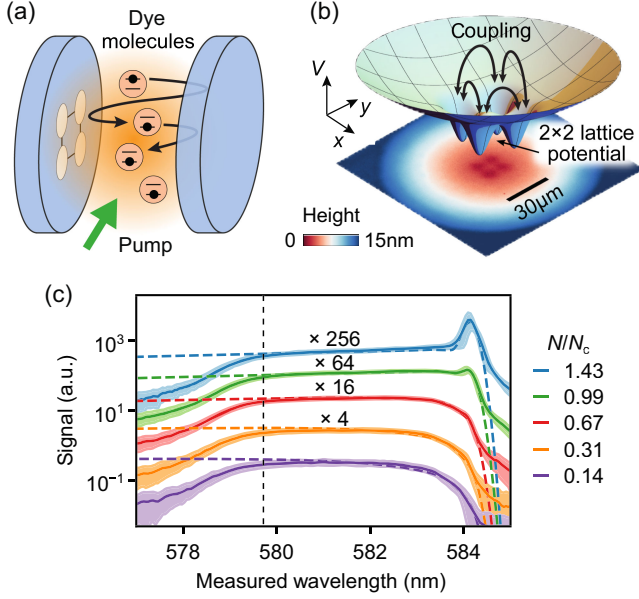
FIG. 1. (a) Experimental scheme of dye-filled optical micro-cavity formed by a microstructured and a plane mirror. The confined photon gas thermalizes by absorption and re-emission processes on dye molecules. (b) Potential experienced by the photons in the cavity (top), as induced by the structured mirror surface (bottom). The coupling between neighboring sites realizes a four-site ring lattice with hybridized eigenstates. (c) Spectral distributions of the thermalized photon gas for increasing N/N_c along with theoretical Bose-Einstein spectra (dashed lines) that take into account the measured mode densities and spectrometer resolution. The finite depth of the imprinted potential is indicated by the black dashed line. Standard deviations are shown as shading.

concentration in ethylene glycol (refractive index $\tilde{n} \approx 1.44$). The microcavity length $D_0 \approx 1.8$ μm is in the wavelength regime, which results in a longitudinal mode spacing sufficiently large that only a single longitudinal mode, with mode number $q = 9$, is populated. This makes the photon gas effectively two-dimensional, introduces a low-frequency cutoff near $\hbar\omega_c \approx 2.1$ eV, with Planck's reduced constant $\hbar$, and the dispersion becomes quadratic. To implement a four-site ring lattice potential superimposed with a harmonic trap, one of the two cavity mirrors is microstructured. For this, a position-dependent local surface elevation is imprinted on the reflecting mirror surface; see Fig. 1(b). Inside the assembled microcavity the elevation leads to a locally repulsive potential, as understood from the shorter wavelength (higher frequency) of the photons required to match the cavity boundary conditions at the corresponding elevated transverse position [22,29]. Accounting for the boundary condition for the longitudinal wave vector component $k_z = q\pi/\{\tilde{n}[D_0 - d(x,y)]\}$ imposed by the mirrors, where $d(x,y)$ denotes the position-dependent mirror elevation and $d(x,y) \ll D_0$, the eigensolutions of photons in the resonator are in paraxial approximation determined by the effective two-dimensional

Hamiltonian [9,22]

$$\hat{H}_{x,y} = m_{\mathrm{ph}} \left(\frac{c}{\tilde{n}}\right)^2 - \frac{\hbar^2}{2m_{\mathrm{ph}}}(\nabla_x^2 + \nabla_y^2) + V(x,y), \quad (1)$$

noting that interactions are weak. Here, c denotes the speed of light, $m_{\mathrm{ph}} = \pi\hbar q\tilde{n}/(cD_0) = \hbar\omega_c(\tilde{n}/c)^2$ an effective photon mass, and $V(x,y) = m_{\mathrm{ph}}(c/\tilde{n})^2 d(x,y)/D_0$ the imprinted trapping potential. Correspondingly, the photon gas in the cavity is formally equivalent to a two-dimensional gas of massive bosons subject to the potential $V(x,y)$. Thermalization of photons to the rovibrational temperature of the dye [19], which is at room temperature, is achieved by repeated absorption re-emission processes on the dye molecules provided the photon lifetime in the cavity is sufficient [30,31]. To inject an initial photon population and compensate for photon loss from, e.g., mirror transmission, the dye microcavity is quasicontinuously pumped with a laser beam at 532 nm wavelength and 55 μm diameter (FWHM).

We model the four-site system using an ansatz for the (scalar) wave function of photon eigenstates $\psi(x,y) = \sum_i c_i \varphi^{(i)}(x,y)$, where the $\varphi^{(i)}(x,y) = \varphi(x - x_i, y - y_i)$ denote localized wave functions and the c_i probability amplitudes, with the index i numbering the sites. The coupling between sites leads to a hybridization of the localized wave functions. The eigensolutions of photons in the lattice can straightforwardly be evaluated by diagonalization of the effective Hamiltonian

$$\hat{H}_{\mathrm{lat}} \simeq \begin{pmatrix} E_s & -J & 0 & -J \\ -J & E_s & -J & 0 \\ 0 & -J & E_s & -J \\ -J & 0 & -J & E_s \end{pmatrix}. \quad (2)$$

The four-component Hamiltonian acts on spinors $\psi = (c_1, c_2, c_3, c_4)$. Here, E_s denotes the localized wave function's eigenenergy, and we only account for the coupling J between neighboring sites, with $J = \langle \varphi^{(i)}|\hat{H}|\varphi^{(i\pm1)}\rangle$, and use a cyclic notation ($\varphi^{(1)} \equiv \varphi^{(5)}$). A set of eigenstates, each of them possessing a twofold polarization degeneracy, can now be written in the form $\psi_\ell = \frac{1}{2}(\varphi^{(1)} + e^{i(\pi/2)\ell}\varphi^{(2)} + e^{i\pi\ell}\varphi^{(3)} + e^{i(3\pi/2)\ell}\varphi^{(4)})$ that is ordered by the phase winding of the four-site quantum ring with $\ell = 0, \pm 1, 2$. Specifically, for $\ell = 0$, the system ground state at energy $E_s - 2J (\equiv \hbar\omega_c)$ is the symmetric linear combination $\psi_0 = \frac{1}{2}(\varphi^{(1)} + \varphi^{(2)} + \varphi^{(3)} + \varphi^{(4)})$, and the excited states of the lattice $\psi_{\pm1}$ and ψ_2 have the energies E_s and $E_s + 2J$, respectively.

Experimentally, the ring potential for the photons described by Eq. (2) is realized by imprinting a surface profile with four indents spaced by roughly 10 μm onto one of the cavity mirrors [29]; see Fig. 1(b). The indents each

exhibit a width of 6.7 μm (FWHM) and a depth of 0.8 nm, which yields a ground state energy close to the potential energy of the barrier separating nearest-neighbor lattice sites but below the potential barrier located in the trap center [32]. The coupling between neighboring sites, as determined spectroscopically, reaches $J \approx h \times 25$ GHz. The lattice potential is superimposed by a harmonic trap with angular frequency $\Omega = c/(\tilde{n}\sqrt{D_0 R}) \approx 2\pi \times 64$ GHz, as realized by additionally imprinting a spherical curvature with a radius of curvature of $R \approx 14.8$ cm on top of the lattice indent structure. The mode density of the harmonic trap is required to enables Bose-Einstein condensation of photons in the two-dimensional system [22].

We first verify the thermalized nature of the photon gas in the combined harmonic and four-site ring potential, being a prerequisite for Bose-Einstein condensation. For this, we have recorded broadband spectra (spectrometer resolution 300 GHz) for different photon numbers; see Fig. 1(c). The spectrometer allows us to record the spectral distribution of the photon gas over the entire trap depth of the harmonic potential. The data is in good agreement with the theory expectation for a Bose-Einstein distribution at $T = 300$ K over the spectral range from 584.1 nm (corresponding to the low-frequency cutoff) to 579.7 nm, at which the finite trap depth of the imprinted potential of approximately $0.63 \times k_B T \approx h \times 3.9$ THz is reached. The data provides a first line of evidence for the thermalization of photons in the tailored potential, which will be complemented by measurements of the spatial intensity distributions in the following; see Fig. 3. While at low photon numbers a Boltzmann distribution is observed, for photon numbers exceeding a critical number $N_c \approx 2780$ a macroscopic occupation of the low-energy modes is evident.

In order to shed more light onto the observed macroscopic occupation, we recorded spectral distributions of the low-energy photons using a highly resolving spectrometer (resolution 20 GHz); the used spectrometer allows us to resolve the lower energetic part of the transverse mode spectrum and extract the state populations. Figure 2(a) shows typical experimental data for photon numbers below and above the Bose-Einstein condensation threshold, respectively. As we use a slitless spectrometer, the dispersed cavity emission still contains information on the spatial mode profile. Along the spectrally dispersed direction (x axis), a cylindrical telescope with a 6∶1 aspect ratio reduces the imaging scale correspondingly. The spatial mode profile along the y axis is visible, for example, for the longest wavelength (lowest photon energy) mode with a profile resembling the symmetric ground state ψ_0 of the ring system, while in the spatial distribution of the third mode a pronounced minimum near $y = 0$ (as well as a minimum along x) is observed, as expected for the antisymmetric state ψ_2. The signal observed at the intermediate wavelength is attributed to the degenerate states $\psi_{\pm 1}$, and the observed spectrum confirms their degeneracy
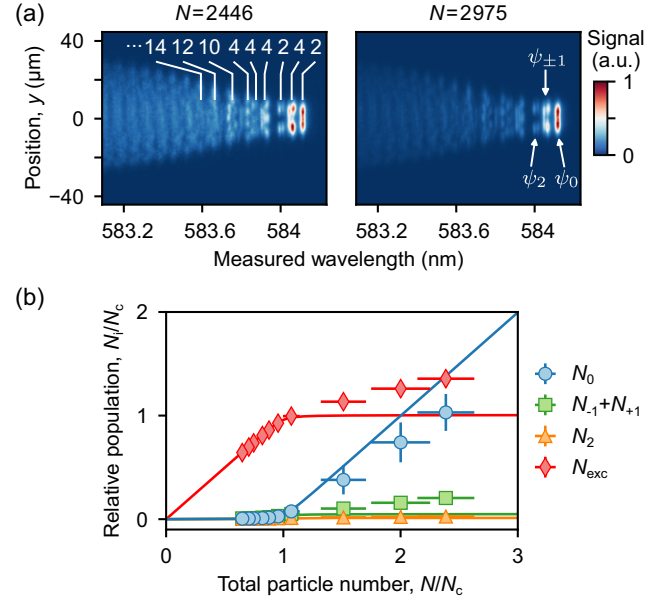

FIG. 2. (a) Spectrally highly resolved data (normalized) showing the distribution of the microcavity emission as a function of the measured wavelength and position along the y axis, corresponding to one of the lattice axes, for $N/N_c = 0.88(3)$ (left panel) and $N/N_c = 1.07(7)$ (right); numbers in the left panel give the mode degeneracy determined independently by exciting the transverse modes with a focused laser beam. The three rightmost spectral lines (at largest wavelengths) correspond to the four ring modes (see arrows), while signals at smaller wavelengths correspond to harmonic oscillator ones. For the large photon number, the Bose-Einstein condensate is seen in the increased emission from the lowest energy state. (b) Relative population in the resolved ring eigenstates N_0, $N_{-1} + N_{+1}$, and N_2, as well as in all available excited states $N_{exc} = N - N_0$ (symbols) versus total photon number along with theory (lines). All numbers are normalized by N_c. Error bars give standard statistical errors; the cutoff wavelength is at 584.1 nm.

within our experimental accuracy. The measured frequency splitting of the hybridized eigenstates ψ_0 and $\psi_{\pm 1}$ or $\psi_{\pm 1}$ and ψ_2 is 48.5(4) GHz and 50.4(9) GHz, respectively. These values are below the theoretically expected splittings for the mirror surface profile, which we have determined independently using white-light interferometry [29,32]. For the next higher energetic modes, we find that their wavelengths and degeneracies cannot be fully described by harmonic oscillator modes. This behavior is well understood from the influence of the lattice potential still being relevant for the energetically lowest-lying harmonic oscillator states. For energies of more than $h \times 400$ GHz above the cutoff, the levels become essentially equidistantly spaced and the mode degeneracy increases linearly, corresponding to the expectations for the harmonic oscillator case of $g(u) = 2(1 + u/\hbar\Omega)$, where u denotes the energy above the cutoff.

To obtain quantitative insight into the behavior at the phase transition, Fig. 2(b) shows the relative population in
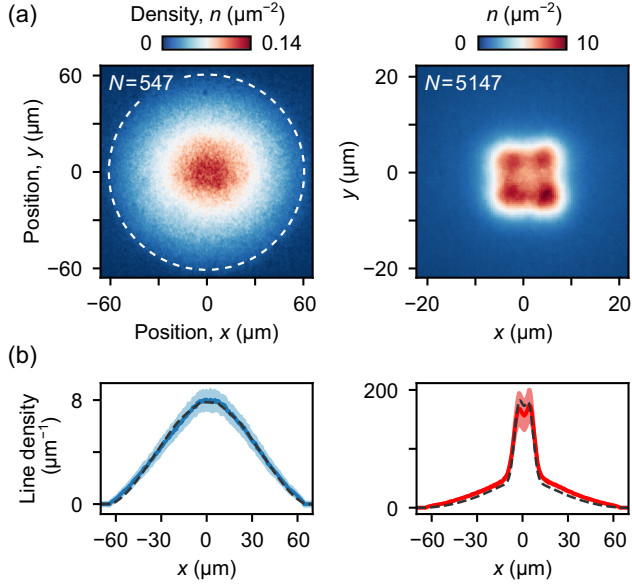
FIG. 3. (a) Density distribution of the photon gas in the microcavity both below (left panel) and above (right) the Bose-Einstein condensation threshold. For $N/N_c = 0.20(2)$, one observes a rotationally symmetric thermal distribution, while for $N/N_c = 1.8(3)$, the fourfold symmetry of the lattice becomes visible as attributed to the dominant contribution by the symmetric ground state $|\psi_0|^2$. Dashed circle indicates the radial extent of the finite-depth harmonic trap. (b) Line densities obtained from integration along the vertical axis of the distributions shown in (a), along with fits based on room-temperature Bose-Einstein distributions (dashed lines), yielding $N = 510(40)$ and $N = 4200(200)$ as fit parameters. Standard deviations are shown as shading.

the low-energy eigenstates of the ring lattice for different photon numbers. Around N_c the ground state population N_0 features a clear threshold behavior, which is revealed by a sudden increase of N_0 with increasing total particle number. Because of the finite size of the system, this phase transition is softened, and correspondingly we determined N_c by a linear fit to the data at large photon numbers. The saturation of the excited mode population N_{exc} expected for a Bose-Einstein condensate is to good approximation fulfilled. Indeed, the dominant contribution to the residual growth of N_{exc} in the condensed regime results largely from the degenerate pair of lattice modes $\psi_{\pm 1}$, as is clearly observed in Fig. 2(b). This behavior is attributed mainly to an incomplete equilibration of the photon gas due to the driven-dissipative nature of the system [41].

The condensation is also revealed in the spatial distribution of the photon gas obtained by imaging the emission from the microcavity plane onto a camera. Experimental data for photon numbers corresponding to below and above N_c is shown in Fig. 3(a). For the data taken in the uncondensed regime [Fig. 3(a), left panel], we observe a broad thermal distribution up to the high-energy edge of the imprinted harmonic potential, which is radially located in

60 μm distance from the trap center. Above the critical photon number [Fig. 3(a), right panel], we observe a four-peaked intensity distribution in the center on top of the thermal cloud, indicating the macroscopic occupation of photons in the symmetric superposition state ψ_0 upon Bose-Einstein condensation. The spatial intensity profile of the populated ground state shows a slight asymmetry among the four lattice sites, which is attributed to residual detunings between the bare eigenenergies caused by height variations of the imprinted potentials below 1 Å [29]. Figure 3(b) shows corresponding line densities obtained from integration along the vertical axes in Fig. 3(a), along with theory based on a Bose-Einstein distributed occupation of the modes bound in the finite-depth potential. The deviation between the measured photon numbers and the fitted ones are attributed to an imperfect saturation of the excited mode population [as previously seen in Fig. 2(b)]. Following the spectroscopic confirmation, the agreement of the measured spatial profiles with the theory prediction gives a second line of evidence for the thermalization of the two-dimensional photon gas.

The four hybridized eigenstates can be uniquely characterized by their corresponding relative phase between the localized lattice site eigenfunctions. To verify the expected phase coherence among the different lattice sites, we perform optical interferometry of the cavity emission. As shown in Fig. 4(a), the cavity output was split into four paths and subsequently recombined, each offset by approximately half the image size, giving access to two- and four-site interference in different spatial regions of the recorded interference pattern. Figure 4(b) shows typical false-color images obtained by imaging the interferometer output on a camera for $N < N_c$ (left panel) and $N > N_c$ (right), respectively. While below the condensation threshold no interference signal is visible, above the condensation threshold a clear interference signal is visible in the regions where the emission of two or more sites spatially overlap. Given that the image is the average of data recorded in many subsequent realizations of the experiment, this confirms the existence of a stable phase relation between the optical fields at different sites. The presence of this fringe pattern confirms their coherence, indicating that a macroscopic wave function extends over all four lattice sites; in other words, a photon is delocalized over the entire ring lattice structure. The visible interference contrast here sets an upper limit to the "which-path" information (here better termed as "which-site information") occurring in the process of thermalization by contact to the dye molecules. For the parameters used in our experiment, the characteristic timescale for photons moving between sites $(h\pi/(2J) \approx 10$ ps) is much shorter than that for dye-mediated thermalization ≈ 130 ps [31], so that the presence of a fringe pattern is well within expectations even in the presence of the coupling to a thermal bath.
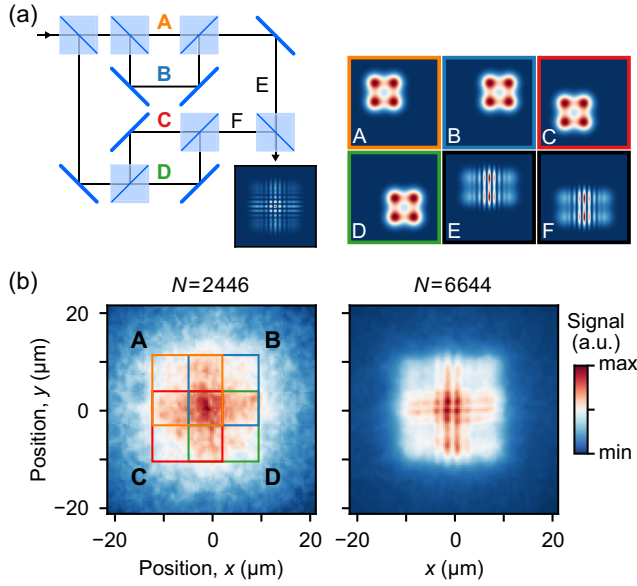
FIG. 4. (a) Interferometry setup to probe the mutual phase coherence of photons from different lattice sites. By spatially overlapping the fields emitted from different transverse points in the cavity, interference signals between two and four sites are recorded. The images on the right show calculated intensity contributions (for pure condensates) from the individual paths A–D, as well as their expected intensity along path E and F. (b) Interference signal below (left) and above (right) the critical photon number for Bose-Einstein condensation with $N/N_c = 0.88(3)$ and $N/N_c = 2.4(2)$, respectively. As in (a), the boxes indicate how the four paths A-D are overlapped in the detector plane; note that the corresponding wave vectors are deliberately tilted to obtain a visible fringe pattern. For the data recorded in the condensed phase, a stable interference signal is visible in regions where the emission from different sites overlap.

To conclude, we have demonstrated Bose-Einstein condensation of photons into the hybridized ground state of a ring lattice. The observed spatial and spectral distributions are in good agreement with equilibrium theory, confirming that the macroscopic state preparation is driven by quantum statistics, in contrast to classical optical state preparation methods where photon loss is balanced by gain. Further, the fixed phase relation of the photons at the different sites of the ring lattice was verified interferometrically.

For the future, lattices of interacting photons induced, e.g., by effective Kerr nonlinearities offer prospects for the preparation of entangled many-body ground states using the demonstrated thermal equilibrium process [22,42]. Combining this approach with reversible thermo-optic methods will enable also the control of spatially extended lattice systems [24,43,44]. The realized quantum ring furthermore holds promise for the engineering of optical analogs of superconducting flux qubits [45]. Other prospects include the "cooling" into low-energy topological states of light based on circular modulations of the tunneling [46], or in a classical regime, simulations of the XY model [20,47].

[1] A. M. Chang, Chiral Luttinger liquids at the fractional quantum Hall edge, Rev. Mod. Phys. **75**, 1449 (2003).

[2] V. V. Deshpande, M. Bockrath, L. I. Glazman, and A. Yacoby, Electron liquids and solids in one dimension, Nature (London) **464**, 209 (2010).

[3] M. Greiner, O. Mandel, T. Esslinger, T. W. Hänsch, and I. Bloch, Quantum phase transition from a superfluid to a Mott insulator in a gas of ultracold atoms, Nature (London) **415**, 39 (2002).

[4] L. Bao, N.-H. Kim, L. J. Mawst, N. N. Elkin, V. N. Troshchieva, D. V. Vysotsky, and A. P. Napartovich, Near-diffraction-limited coherent emission from large aperture antiguided vertical-cavity surface-emitting laser arrays, Appl. Phys. Lett. **84**, 320 (2004).

[5] M. Nixon, E. Ronen, A. A. Friesem, and N. Davidson, Observing geometric frustration with thousands of coupled lasers, Phys. Rev. Lett. **110**, 184102 (2013).

[6] H. Deng, H. Haug, and Y. Yamamoto, Exciton-polariton Bose-Einstein condensation, Rev. Mod. Phys. **82**, 1489 (2010).

[7] I. Carusotto and C. Ciuti, Quantum fluids of light, Rev. Mod. Phys. **85**, 299 (2013).

[8] J. Klaers, J. Schmitt, F. Vewinger, and M. Weitz, Bose–Einstein condensation of photons in an optical microcavity, Nature (London) **468**, 545 (2010).

[9] J. Schmitt, Dynamics and correlations of a Bose–Einstein condensate of photons, J. Phys. B **51**, 173001 (2018).

[10] J. Bloch, I. Carusotto, and M. Wouters, Non-equilibrium Bose–Einstein condensation in photonic systems, Nat. Rev. Phys. **4**, 470 (2022).

[11] J. Marelic and R. A. Nyman, Experimental evidence for inhomogeneous pumping and energy-dependent effects in photon Bose-Einstein condensation, Phys. Rev. A **91**, 033813 (2015).

[12] S. Greveling, K. L. Perrier, and D. van Oosten, Density distribution of a Bose-Einstein condensate of photons in a dye-filled microcavity, Phys. Rev. A **98**, 013810 (2018).

[13] M. Vretenar, C. Toebes, and J. Klaers, Modified Bose-Einstein condensation in an optical quantum gas, Nat. Commun. **12**, 5749 (2021).

[14] R. Weill, A. Bekker, B. Levit, and B. Fischer, Bose–Einstein condensation of photons in an erbium–ytterbium co-doped fiber cavity, Nat. Commun. **10**, 747 (2019).

[15] T. K. Hakala, A. J. Moilanen, A. I. Väkeväinen, R. Guo, J.-P. Martikainen, K. S. Daskalakis, H. T. Rekola, A. Julku, and P. Törmä, Bose–Einstein condensation in a plasmonic lattice, Nat. Phys. **14**, 739 (2018).

[16] R. C. Schofield, M. Fu, E. Clarke, I. Farrer, A. Trapalis, H. S. Dhar, R. Mukherjee, J. Heffernan, F. Mintert, R. A. Nyman, and R. F. Oulton, Bose-Einstein condensation of light in a semiconductor quantum well microcavity, Nat. Photon. (2024).

[17] M. Pieczarka, M. Gębski, A. N. Piasecka, J. A. Lott, A. Pelster, M. Wasiak, and T. Czyszanowski, Bose-Einstein condensation of photons in a vertical-cavity surface-emitting laser, Nat. Photon. (2024).

[18] J. L. Figueiredo, J. T. Mendonça, and H. Terças, Bose-Einstein condensation of photons in microcavity plasmas, Phys. Rev. E **108**, L013201 (2023).

[19] J. Klaers, J. Schmitt, T. Damm, F. Vewinger, and M. Weitz, Statistical physics of Bose-Einstein-condensed light in a dye microcavity, Phys. Rev. Lett. **108**, 160403 (2012).

[20] N. G. Berloff, M. Silva, K. Kalinin, A. Askitopoulos, J. D. Töpfer, P. Cilibrizzi, W. Langbein, and P. G. Lagoudakis, Realizing the classical XY Hamiltonian in polariton simulators, Nat. Mater. **16**, 1120 (2017).

[21] I. Gershenzon, G. Arwas, S. Gadasi, C. Tradonsky, A. Friesem, O. Raz, and N. Davidson, Exact mapping between a laser network loss rate and the classical XY Hamiltonian by laser loss control, Nanophotonics **9**, 4117 (2020).

[22] C. Kurtscheid, D. Dung, E. Busley, F. Vewinger, A. Rosch, and M. Weitz, Thermally condensing photons into a coherently split state of light, Science **366**, 894 (2019).

[23] T. Jacqmin, I. Carusotto, I. Sagnes, M. Abbarchi, D. D. Solnyshkov, G. Malpuech, E. Galopin, A. Lemaître, J. Bloch, and A. Amo, Direct observation of Dirac cones and a flatband in a honeycomb lattice for polaritons, Phys. Rev. Lett. **112**, 116402 (2014).

[24] M. Vretenar, B. Kassenberg, S. Bissesar, C. Toebes, and J. Klaers, Controllable Josephson junction for photon Bose-Einstein condensates, Phys. Rev. Res. **3**, 023167 (2021).

[25] P. G. Lagoudakis and N. G. Berloff, A polariton graph simulator, New J. Phys. **19**, 125008 (2017).

[26] S. Mukherjee, D. M. Myers, R. G. Lena, B. Ozden, J. Beaumariage, Z. Sun, M. Steger, L. N. Pfeiffer, K. West, A. J. Daley, and D. W. Snoke, Observation of nonequilibrium motion and equilibration in polariton rings, Phys. Rev. B **100**, 245304 (2019).

[27] S. Mukherjee, V. K. Kozin, A. V. Nalitov, I. A. Shelykh, Z. Sun, D. M. Myers, B. Ozden, J. Beaumariage, M. Steger, L. N. Pfeiffer, K. West, and D. W. Snoke, Dynamics of spin polarization in tilted polariton rings, Phys. Rev. B **103**, 165306 (2021).

[28] J. Wang, H. Xu, R. Su, Y. Peng, J. Wu, T. C. Liew, and Q. Xiong, Spontaneously coherent orbital coupling of counter-rotating exciton polaritons in annular perovskite microcavities, Light Sci. Appl. **10**, 45 (2021).

[29] C. Kurtscheid, D. Dung, A. Redmann, E. Busley, J. Klaers, F. Vewinger, J. Schmitt, and M. Weitz, Realizing arbitrary trapping potentials for light via direct laser writing of mirror surface profiles, Europhys. Lett. **130**, 54001 (2020).

[30] P. Kirton and J. Keeling, Thermalization and breakdown of thermalization in photon condensates, Phys. Rev. A **91**, 033826 (2015).

[31] J. Schmitt, T. Damm, D. Dung, F. Vewinger, J. Klaers, and M. Weitz, Thermalization kinetics of light: From laser dynamics to equilibrium condensation of photons, Phys. Rev. A **92**, 011602(R) (2015).

[32] See Supplemental Material at http://link.aps.org/supplemental/10.1103/PhysRevLett.133.093602 for details on experimental and theoretical methods, which includes Refs. [33–40].

[33] B. I. Stepanov and L. P. Kazachenko, Universal relationship between absorption and emission spectra taking the solvent effect into account, J. Appl. Spectrosc. **14**, 596 (1971).

[34] J. Lakowicz, *Principles of Fluorescence Spectroscopy* (Springer, New York, NY, 2006).

[35] H. Yokoyama and S. D. Brorson, Rate equation analysis of microcavity lasers, J. Appl. Phys. **66**, 4801 (1989).

[36] J. Klaers, J. Schmitt, T. Damm, F. Vewinger, and M. Weitz, Bose-Einstein condensation of paraxial light, Appl. Phys. B **105**, 17 (2011).

[37] P. Kirton and J. Keeling, Nonequilibrium model of photon condensation, Phys. Rev. Lett. **111**, 100404 (2013).

[38] G. Gioia and M. Ortiz, *Delamination of Compressed Thin Films* (Elsevier, New York, 1997), pp. 119–192.

[39] S. Greveling, F. van der Laan, H. C. Jagers, and D. van Oosten, Polarization of a Bose-Einstein condensate of photons in a dye-filled microcavity, arXiv:1712.08426.

[40] R. I. Moodie, P. Kirton, and J. Keeling, Polarization dynamics in a photon Bose-Einstein condensate, Phys. Rev. A **96**, 043844 (2017).

[41] J. Keeling and P. Kirton, Spatial dynamics, thermalization, and gain clamping in a photon condensate, Phys. Rev. A **93**, 013829 (2016).

[42] A. Majumdar and D. Gerace, Single-photon blockade in doubly resonant nanocavities with second-order nonlinearity, Phys. Rev. B **87**, 235319 (2013).

[43] D. Dung, C. Kurtscheid, T. Damm, J. Schmitt, F. Vewinger, M. Weitz, and J. Klaers, Variable potentials for thermalized light and coupled condensates, Nat. Photonics **11**, 565 (2017).

[44] E. Busley, L. E. Miranda, A. Redmann, C. Kurtscheid, K. K. Umesh, F. Vewinger, M. Weitz, and J. Schmitt, Compressibility and the equation of state of an optical quantum gas in a box, Science **375**, 1403 (2022).

[45] Y. Xue, I. Chestnov, E. Sedov, E. Kiktenko, A. K. Fedorov, S. Schumacher, X. Ma, and A. Kavokin, Split-ring polariton condensates as macroscopic two-level quantum systems, Phys. Rev. Res. **3**, 013099 (2021).

[46] K. Fang, Z. Yu, and S. Fan, Realizing effective magnetic field for photons by controlling the phase of dynamic modulation, Nat. Photonics **6**, 782 (2012).

[47] V. N. Gladilin and M. Wouters, Vortices in nonequilibrium photon condensates, Phys. Rev. Lett. **125**, 215301 (2020).